Sound & Vibration 2026, 60(5), 4626.
doi: https://doi.org/10.59400/sv4626

Article

Alpha-cut robust design of a fractional-order fuzzy tuned mass damper for targeted-band vibration suppression in rotating machinery

Yogeesh Nijalingappa[1,2,3,*], Asokan Vasudevan[3], Tahir Muhammad Ali[4], Rajashree Jain[5], P. William[6,7]

[1] Department of Mathematics, Government First Grade College, Tumkur 572102, India
[2] Mathematics and Natural Sciences, Gulf University for Science and Technology, Safat 13060, Kuwait
[3] Faculty of Business and Communications, INTI International University, Nilai 71800, Malaysia
[4] Department of Computer Science, Gulf University for Sciences and Technology, Safat 13060, Kuwait
[5] Symbiosis Institute of Computer Studies and Research, Symbiosis International (Deemed University), Pune 411016, India
[6] School of Computer Science and Technology, Karunya Institute of Technology and Sciences (Deemed University), Coimbatore 641114, India
[7] Centre for Research and Consultancy, UNITAR International University, Petaling Jaya 47301, Malaysia
*** Corresponding author:** Yogeesh Nijalingappa, yogeesh.n@ka.gov.in

CITATION

Nijalingappa Y, Vasudevan A, Ali TM, et al. Alpha-cut robust design of a fractional-order fuzzy tuned mass damper for targeted-band vibration suppression in rotating machinery. Sound & Vibration. 2026; 60(5): 4626. https://doi.org/10.59400/sv4626

ARTICLE INFO

Received: 6 July 2026
Revised: 16 July 2026
Accepted: 27 July 2026
Available online: 16 August 2026

Abstract: This study presents a targeted-band design method for suppressing flexible-rotor vibration using a fractional-order fuzzy tuned mass damper. A force-excited rotor-support mode represents the host machine, while the absorber branch comprises a spring and fractional dashpot. The absorber parameters are selected to minimize the primary displacement peak while remaining robust to bounded uncertainty in mass ratio, tuning ratio, damping index, fractional order, support stiffness, and force level. Triangular fuzzy numbers are propagated through alpha-cut intervals, and the resulting frequency-response envelopes are optimized by a weighted objective that penalizes high peaks and wide uncertainty spreads. Closed-form frequency-response relations evaluated directly at interval corners keep the procedure transparent and reproducible. For a rotor-support oscillator with natural frequency 9.762 Hz, primary mass 42 kg, primary stiffness 158,000 N/m, force amplitude 58 N, and mass ratio $\mu = 0.05$, the optimized design yields a central peak displacement of 1.929 mm and an alpha-zero upper peak of 3.154 mm, compared with 10.197 mm for the uncontrolled system and 2.028 mm for the deterministic Den Hartog reference. Evaluation at $\mu = 0.03$, 0.05, and 0.07 shows consistent peak reduction and useful trends for initial parameter tuning. The method therefore provides bounded vibration envelopes, tuning guidance, stroke estimates, and sensitivity rankings for uncertain rotating-machine data within the specified target band.

Keywords: fractional damping; alpha-cut; robust tuned mass damper; interval response; rotating machinery

1. Introduction

Active absorbers, while requiring less restriction on the tuning frequency ready, have fallen out of favor with rotating machinery users due to their need for external power sources, and difficulty of maintenance after the fundamental mode has been established (in cases where systems are not remote-controlled). This is why classical tuned mass dampers are so frequently employed, however the performance of these systems can be sensitive to mistuning. For example, a moderate 10% frequency mismatch in the absorbers, loss factor or support stiffness can disrupt the preferred split-peak balance and eliminate almost half of expected attenuation. This limitation is well known in the structural dynamics and vibration control community. Simultaneously, real machine data is often sparse: a designer may know a nominal support stiffness, a nominal absorber mass and target speed range, yet not unique exact values for all parameters. This scenario is suitable for fuzzy mathematics, because bounded engineering vagueness can be represented directly by using of fuzzy sets and possibility theory [1–5], while the transformation and fuzzy finite-element methods have already demonstrated a framework [6–10] in which epistemic uncertainty can propagate to structural response analysis [11,12].

The literature offers three ingredients that motivate this research work [1–5]. The first ingredient is the fuzzy-analysis framework based on triangular fuzzy magnitudes, alpha-cuts and transformation procedures [6–10], which has been used for fuzzy frequency response functions and explicit interval propagation in structural dynamics [11,12]. The second ingredient is robust absorber design under uncertain parameters, where the best nominal absorber may not be the best practical absorber once tolerances are included [13]. The third ingredient is the recent growth of inerter-enhanced and fractional-order damping concepts in vibration engineering [14–18]. Inerter devices enlarge the passive design space [19–23], whereas fractional operators provide compact frequency-dependent storage and loss terms for viscoelastic, electromagnetic and smart-material damping elements [21–25].

Recent studies also show that tuned mass damper technology is moving from purely deterministic formulas toward optimization, reliability and adaptive absorber concepts [26–30]. State-of-the-art reviews identify TMD simplicity and reliability as major advantages, but also stress the sensitivity of classical tuning to the selected design frequency [31]. Reliability-based and reliability-informed TMDI studies demonstrate that absorber performance should be judged not only by a nominal peak but also by the response dispersion under uncertain seismic or mechanical inputs [28,32,33]. Recent fractional and delayed resonator models further confirm that the fractional order can be treated as a tunable design variable for shaping damping and stiffness over a frequency band [34–37]. However, these strands are usually developed separately. A compact alpha-cut formulation that combines fractional impedance, fuzzy design variables and a directly auditable robust objective for rotating-machine support modes remains limited in the available literature.

In this present study, we take a single dominant support mode of a rotating machine, attach a secondary absorber, and let the absorber damper be fractional-order. The central design variables are then the mass ratio, tuning ratio, fractional damping index, and fractional order. Instead of treating them as fixed scalars, we represent them as fuzzy numbers. Our primary job is to calculate on a speed band the displacement envelope of the grounded mass and setting the nominal absorb used, so that worst peak remain smaller, along with narrow fuzzy spread. Thus it marries a classical absorber problem with fuzzy arithmetic, in a format amenable to tabulation, optimization and direct interpretation.

The current work is intentionally mathematical in its organization: first, the deterministic harmonic-balance equations are expressed and then transformed into a concise dimensionless frequency-response equation. Each uncertain parameter transforms to an alpha-cut interval, and the response envelope incorporates at each alpha level based on a corner problem solution over the Cartesian product of interval endpoints. The solution defined over a practical design grid is to minimize a weighted robust objective. This sequence keeps the final design problem transparent, and every number in the tables can be traced back to a closed-form dynamic-stiffness expression.

The main contribution is not a new hardware concept, but an integrated fuzzy-fractional design route. The route outputs guaranteed and optimistic frequency-response bands, optimum nominal absorber settings for several mass ratios, contraction of the fuzzy peak as alpha increases, and a local sensitivity ranking of the design variables. It also provides direct surrogate relations for the optimum tuning quantities, so that an engineer can obtain a useful starting design without repeating the full search [13,31–34,38,39].

The novel contributions of this work are fourfold. First, a fractional-order tuned mass damper is embedded in an alpha-cut fuzzy design framework for a rotating-machine support mode. Second, all dominant uncertain quantities are treated as triangular fuzzy numbers, allowing both optimistic and guaranteed response envelopes to be obtained in the same calculation chain. Third, a weighted objective combines worst-case peak control with fuzzy-spread reduction and stroke awareness. Fourth, the numerical results are interpreted through mass-ratio trends, alpha-cut contraction and normalized sensitivity measures rather than through a single deterministic response curve.

2. Deterministic primary-absorber model

2.1. Governing equations

The lumped coordinates $x(t)$ and $y(t)$ are the absolute displacements of the dominant machine-support mode and the attached absorber, respectively, measured in the same inertial frame. The primary spring and viscous damper connect the primary mass to ground, whereas the absorber spring and fractional dashpot act on the relative displacement $x(t)$–$y(t)$.

Following the classical two-degree-of-freedom absorber formulation and the fractional viscoelastic damping representation [21,34,38], the forced equations are

$$m_p\ddot{x} + c_p\dot{x} + k_p x + k_a(x-y) + c_q D^q(x-y) = F_0 \cos \mathit{\Omega} t \tag{1}$$

$$m_a\ddot{y} + k_a(y-x) + c_q D^q(y-x) = 0 \tag{2}$$

where $D^q(\cdot)$ is a Caputo-type derivative of order $0 < q \leq 1$. The force can be an unbalance loading in a harmonicized model or a narrow-band operational excitation. The goal is to reduce the main displacement amplitude in a specific frequency region surrounding the prevailing support resonance.

We list the key physical constants employed in numerical investigation in **Table 1**.

Table 1. Primary system constants used in the rotor-support example.

Quantity	Value	Unit
Primary mass	42.000	kg
Primary stiffness	158,000.000	N/m
Primary viscous damping ratio	0.018	-
Primary natural circular frequency	61.334	rad/s
Primary natural frequency	9.762	Hz
Harmonic force amplitude	58.000	N
Static reference displacement F0/kp	0.367	mm

For a harmonic steady state, the complex-amplitude representation commonly used in vibration-absorber analysis is written as [31,38]

$$x(t)= \Re\left[Xe^{i\Omega t}\right], \qquad y(t)= \Re\left[Ye^{i\Omega t}\right] \tag{3}$$

and the fractional operator becomes

$$D^q e^{i\Omega t} = (i\Omega)^q e^{i\Omega t}. \tag{4}$$

Therefore,

$$\left[-m_p\Omega^2 + ic_p\Omega + k_p + k_a + c_q(i\Omega)^q\right]X - \left[k_a + c_q(i\Omega)^q\right]Y = F_0 \tag{5}$$

$$-\left[k_a + c_q(i\Omega)^q\right]X + \left[-m_a\Omega^2 + k_a + c_q(i\Omega)^q\right]Y = 0. \tag{6}$$

The determinant of the dynamic stiffness matrix is

$$\begin{aligned}\Delta(\Omega) = \left(-m_p\Omega^2 + ic_p\Omega + k_p + k_a + c_q(i\Omega)^q\right)\left(-m_a\Omega^2 + k_a + c_q(i\Omega)^q\right) \\ - \left(k_a + c_q(i\Omega)^q\right)^2.\end{aligned} \tag{7}$$

Solving the equations of two-by-two system gives the complex amplitudes

$$X(\Omega) = \frac{F_0\left[-m_a\Omega^2 + k_a + c_q(i\Omega)^q\right]}{\Delta(\Omega)} \tag{8}$$

$$Y(\Omega) = \frac{F_0\left[k_a + c_q(i\Omega)^q\right]}{\Delta(\Omega)}. \tag{9}$$

These two equations are the base of the entire this study. Once X and Y are well known, the primary displacement, absorber motion, and also absorber stroke is immediate.

2.2. Dimensionless response relations

To reduce the design space, the standard nondimensional absorber ratios are introduced in the form used in tuned-absorber design [31, 38]. Define the primary natural frequency, the static reference displacement, and the standard ratios as

$$\Omega_p = \sqrt{\frac{k_p}{m_p}}, \qquad x_s = \frac{F_0}{k_p}, \qquad \lambda = \frac{\Omega}{\Omega_p} \tag{10}$$

$$\mu = \frac{m_a}{m_p}, \qquad \nu = \frac{\Omega_a}{\Omega_p}, \qquad \Omega_a = \sqrt{\frac{k_a}{m_a}}, \qquad \zeta_p = \frac{c_p}{2m_p\Omega_p}. \tag{11}$$

The absorber spring is written as

$$k_a = \mu\nu^2 k_p. \tag{12}$$

The fractional dashpot coefficient is nondimensionalized through a fractional damping index ξ_q,

$$c_q = 2\mu\xi_q m_p \Omega_p^{2-q}. \tag{13}$$

With these definitions, the normalized fractional impedance term becomes

$$s_q(\lambda) = 2\mu\xi_q\lambda^q \left[\cos\left(\frac{q\pi}{2}\right) + i\sin\left(\frac{q\pi}{2}\right)\right]. \tag{14}$$

The dimensionless stiffness coefficients are then

$$z_{11} = 1 - \lambda^2 + 2i\zeta_p\lambda + \mu\nu^2 + s_q(\lambda) \tag{15}$$

$$z_{22} = \mu\left(\nu^2 - \lambda^2\right) + s_q(\lambda) \tag{16}$$

$$z_{12} = z_{21} = -\left[\mu\nu^2 + s_q(\lambda)\right]. \tag{17}$$

After division by k_p, the determinant becomes

$$\delta(\lambda) = z_{11}z_{22} - z_{12}^2. \tag{18}$$

The normalized primary amplitude ratio is

$$A(\lambda) = \left|\frac{X}{x_s}\right| = \left|\frac{z_{22}}{\delta(\lambda)}\right|. \tag{19}$$

The normalized absorber amplitude and normalized relative stroke are

$$B(\lambda) = \left|\frac{Y}{x_s}\right| = \left|\frac{-z_{12}}{\delta(\lambda)}\right| \tag{20}$$

$$R(\lambda) = \left|\frac{X - Y}{x_s}\right|. \tag{21}$$

In the present study the design objective is based mainly on $A(\lambda)$ because the machine vibration at the support point is the first quantity of interest. The stroke $R(\lambda)$ is still important because it limits the practical motion range of the auxiliary mass.

2.3. Peak measures and deterministic baseline

For any fixed design vector

$$\theta = (\mu, \nu, \xi_q, q) \tag{22}$$

The deterministic peak measures are defined by

$$P_A(\theta) = \max_{\lambda \in [\lambda_1, \lambda_2]} A(\lambda; \theta) \tag{23}$$

$$P_R(\theta) = \max_{\lambda \in [\lambda_1, \lambda_2]} R(\lambda; \theta). \tag{24}$$

The band used in the calculations is

$$\lambda \in [0.65, 1.45]. \tag{25}$$

This frequency band is sufficiently wide to include the unsuppressed peak, the two split controlled peaks and the off-resonant tails. For reference, the same mass ratio is also set by a deterministic Den Hartog-type rule for a classical viscous absorber with:

$$\nu_{DH} \approx \frac{1}{1+\mu}, \qquad \xi_{DH} \approx \sqrt{\frac{3\mu}{8(1+\mu)}}. \tag{26}$$

The deterministic reference is useful because it provides a compact benchmark based on the classical absorber rule [38]; however, it does not account for fuzzy uncertainty in tuning, damping or support stiffness.

3. Fuzzy parameterization and alpha-cut propagation

3.1. Triangular fuzzy numbers

The uncertain design parameters are represented by triangular fuzzy numbers as per equation below

$$\widetilde{p} = \left(p^L, p^C, p^U\right) \tag{27}$$

with membership function

$$\mu_{\widetilde{p}}(p) = \begin{cases} 0, & p < p^L \\ \frac{p-p^L}{p^C-p^L}, & p^L \le p \le p^C \\ \frac{p^U-p}{p^U-p^C}, & p^C \le p \le p^U \\ 0, & p > p^U. \end{cases} \tag{28}$$

The central value p^C is the nominal design value. and the lower and upper values are practical bounds produces by manufacturing tolerance or engineering judgment. In this study the fuzzy variables are

$$\widetilde{\mu} = (0.92\mu, \mu, 1.08\mu), \qquad \widetilde{\nu} = (0.96\nu, \nu, 1.04\nu), \tag{29}$$

$$\widetilde{\xi}_q = (0.85\xi_q, \xi_q, 1.15\xi_q), \qquad \widetilde{q} = (q - 0.08, q, q + 0.08) \tag{30}$$

with the lower and upper order truncated to the interval $(0.55, 1.0]$ when needed. The support stiffness ratio and the force amplitude ratio are also treated as fuzzy quantities,

$$\widetilde{\kappa} = (0.95, 1.00, 1.05), \qquad \widetilde{\varphi} = (0.96, 1.00, 1.04), \tag{31}$$

where κ multiplies the primary stiffness and φ multiplies the harmonic force. This choice reflects the fact that field measurements often show small but non-negligible uncertainty in support stiffness and excitation level. The selected ranges follow the bounded-tolerance treatment used in fuzzy robust absorber design [13]: ±4% is assigned to controlled tuning and force variation, ±5–8% to support-stiffness and mass uncertainty, and the wider ±15% damping-index and ±0.08 order bounds to greater material and model variability. These values are illustrative rather than universal and should be replaced by measured manufacturing and operating tolerances for a specific machine; the local sensitivity analysis identifies mass ratio and tuning accuracy as the dominant local priorities.

3.2. Alpha-cuts and interval design space

For any triangular fuzzy number, the alpha-cut is the closed interval

$$[p]_\alpha = \left[p^L + \alpha\left(p^C - p^L\right),\ p^U - \alpha\left(p^U - p^C\right)\right], \qquad 0 \le \alpha \le 1. \tag{32}$$

Thus the fuzzy design box at level α is

$$\Gamma_\alpha = [\mu]_\alpha \times [\nu]_\alpha \times [\xi_q]_\alpha \times [q]_\alpha \times [\kappa]_\alpha \times [\varphi]_\alpha. \tag{33}$$

Because the response is nonlinear in the uncertain variables, the primary displacement at each frequency is no longer a single number. It becomes an interval. The lower and upper response envelopes are defined by

$$\underline{A}_\alpha(\lambda) = \min_{\eta \in \Gamma_\alpha} A(\lambda; \eta) \tag{34}$$

$$\overline{A}_\alpha(\lambda) = \max_{\eta \in \Gamma_\alpha} A(\lambda; \eta). \tag{35}$$

Likewise, the lower and upper stroke envelopes are

$$\underline{R}_\alpha(\lambda) = \min_{\eta \in \Gamma_\alpha} R(\lambda; \eta) \tag{36}$$

$$\overline{R}_\alpha(\lambda) = \max_{\eta \in \Gamma_\alpha} R(\lambda; \eta). \tag{37}$$

The study uses the exact corner set of the Cartesian box. For six interval variables the corner set contains $2^6 = 64$ combinations at each alpha level. Since the model is inexpensive, this direct corner search is preferable to a surrogate in the current study.

3.3. Robust objective functional

The upper peak amplitude alone is not enough for a fuzzy design because two absorbers may have similar worst peaks but very different uncertainty widths. We therefore define a weighted robust functional

$$J(\theta) = \sum_{j=1}^{m} w_j \left[\max_\lambda \overline{A}_{\alpha_j}(\lambda) + \rho \max_\lambda \overline{R}_{\alpha_j}(\lambda) + \beta\, \overline{W}_{\alpha_j}\right] \tag{38}$$

with

$$\overline{W}_{\alpha_j} = \frac{1}{N_\lambda} \sum_{k=1}^{N_\lambda} \left[\overline{A}_{\alpha_j} (\lambda_k) - \underline{A}_{\alpha_j} (\lambda_k) \right]. \tag{39}$$

The present calculations use

$$\alpha_j \in \{0, 0.25, 0.50, 0.75, 1.00\}, \qquad w_j = \{0.10, 0.15, 0.20, 0.25, 0.30\}, \tag{40}$$

$$\rho = 0.04, \qquad \beta = 0.35. \tag{41}$$

The increasing weights with alpha place slightly more importance on the central and near-central fuzzy levels, while the alpha-zero support still affects the final design. This is a good compromise when the designer wants a robust nominal setting but does not want the entire design to be driven only by the outermost support box. Five uniformly spaced alpha levels were selected to represent the full support-to-core range while retaining 64 corner evaluations at each level. Monotonicity does not depend on this sampling: for $\alpha_2 > \alpha_1$, $\Gamma\alpha_2 \subset \Gamma\alpha_1$, so the upper envelope cannot increase and the lower envelope cannot decrease at any frequency. The five levels are therefore representative objective and reporting cuts, not a numerical claim about continuous-domain convergence.

A related possibility-style interpretation is also useful. For a target amplitude limit A^*, the condition

$$\overline{A}_0(\lambda) \leq A^* \tag{42}$$

means that the limit is satisfied across the full fuzzy support at that frequency. The condition

$$\underline{A}_1(\lambda) \leq A^* \tag{43}$$

is only the crisp central satisfaction. The alpha family therefore supplies a graded view between central performance and guaranteed support performance. This graded view is one of the reasons fuzzy mathematics is convenient for passive absorber design under incomplete information [1–5, 13].

3.4. Numerical design setting and optimization

The search is performed on the dimensionless grid

$$\mu \in \{0.03, 0.05, 0.07\}, \qquad \nu \in [0.78, 0.98], \tag{44}$$

$$\xi_q \in [0.05, 0.22], \qquad q \in [0.58, 0.98]. \tag{45}$$

The band for optimization is sampled by 180 to 240 frequency points depending on the stage of the search, and the final response curves are computed on a dense grid of 1,000 points. For each fixed mass ratio μ, the design pair (ν, ξ_q, q) that minimizes J is selected. The resulting physical absorber quantities are reconstructed from

$$m_a = \mu m_p \tag{46}$$

$$k_a = \mu \nu^2 k_p \tag{47}$$

$$c_q = 2\mu\xi_q m_p \omega_p^{2-q}. \tag{48}$$

The optimum values obtained from the numerical search are given in **Table 2**.

Table 2. Optimum fuzzy fractional absorber settings and reconstructed physical parameters.

μ	m_a(kg)	$\nu*$	ξ_q*	$q*$	$k_a\left(\frac{N}{m}\right)$	$c_q\left(N\cdot\frac{s^q}{m}\right)$	J_{rob}(mm)	**Central peak (mm)**	**Stroke at α = 1 (mm)**
0.030	1.260	0.879	0.135	0.600	3,659.541	108.492	4.106	2.399	59.732
0.050	2.100	0.841	0.158	0.580	5,583.092	229.586	3.154	1.929	69.069
0.070	2.940	0.800	0.190	0.600	7,078.400	354.882	2.685	1.683	73.673

Note: The superscript asterisk (*) denotes the optimized value of the corresponding design variable.

Three simple observations follow immediately from **Table 2**. First, higher absorber mass reduces the worst peak, but it also requires a stiffer auxiliary spring and a larger fractional damping coefficient. Second, the optimum tuning ratio decreases as the mass ratio grows. Third, the optimum fractional index increases with mass ratio. These trends are compactly summarized by the surrogate relations extracted from the three optimized points:

$$\nu^\star \approx 0.938 - 1.967\mu, \xi_q^\star \approx 0.093 + 1.359\mu, \text{ and } q^\star \approx 50.0\mu^2 - 5.000\mu + 0.705.$$

Here, the superscript star ($\star$) denotes an optimized value.

These fitted expressions are not proposed as universal laws. They are only local design rules for the present machine and the present fuzzy uncertainty level. Still, they are useful because they reduce the initial tuning effort in follow-up designs. The corresponding physical configuration is shown in **Figure 1**.

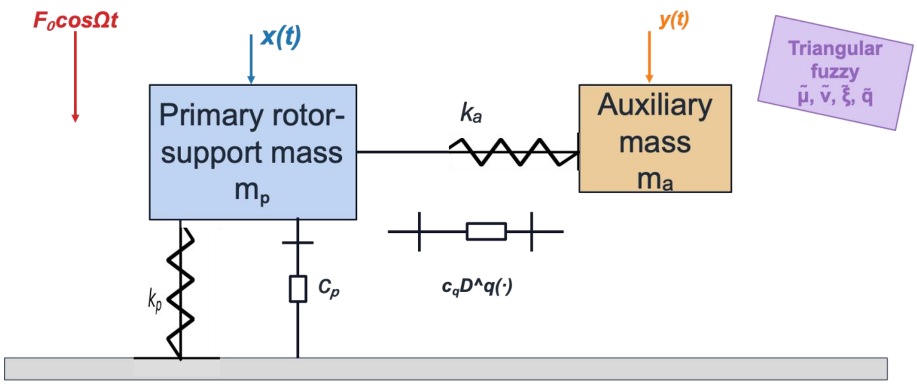

Figure 1. Fractional-order fuzzy TMD attached to a rotor-support oscillator.

4. Results and discussion

4.1. Frequency-response comparison

The first question is simple: how much does the fuzzy robust design reduce the main peak? **Figure 2** answers that question. The uncontrolled system reaches a peak of 10.197 mm. The deterministic Den Hartog reference with the same mass ratio $\mu = 0.05$ reduces the peak to 2.028 mm, which corresponds to a reduction of 80.11%. The fuzzy robust fractional design reduces the central peak further to 1.929 mm, a reduction of 81.08%. More importantly for practice, the alpha-zero support peak is 3.154 mm. That worst-case fuzzy level is still much smaller than the uncontrolled response and remains below one third of the original peak.

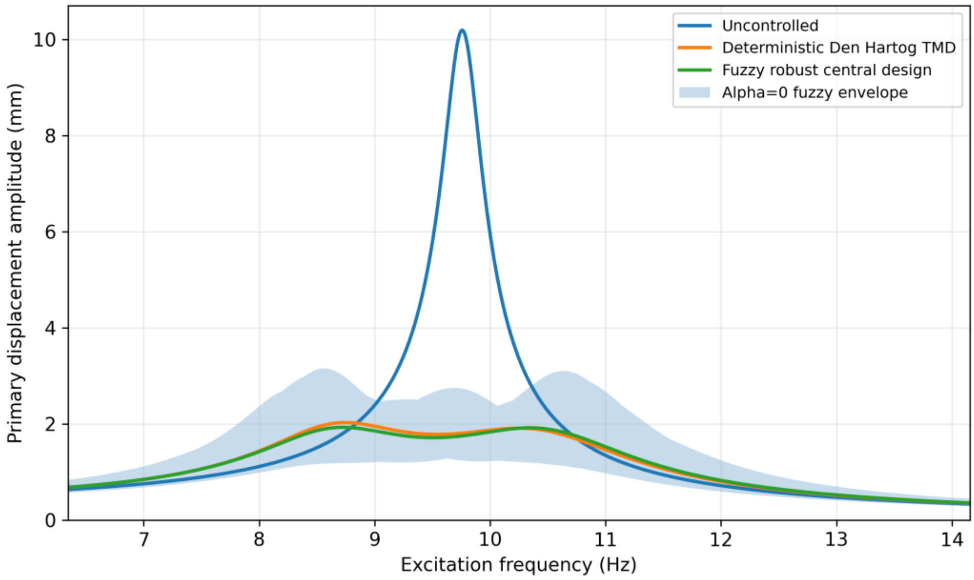

Figure 2. Frequency-response comparison of uncontrolled, deterministic, and fuzzy-robust designs.

The plot also shows a result that is easy to miss if one looks only at a single curve. The alpha-zero fuzzy envelope is wide in the two split-resonance neighborhoods but narrow elsewhere. This means that the uncertainty affects the design mostly through the exact location and balance of the controlled peaks. Outside those narrow neighborhoods the response is much less sensitive. In practical terms, the absorber does not need to be perfect across the entire band. It only needs to remain well balanced near the coupled resonances. This interpretation is in line with standard tuned-absorber theory, but the fuzzy envelope makes it explicit.

Peak levels at the five alpha-cut points are shown in **Table 3**. This reduces the old maximum peak value as alpha increases because the interval box made for index lessens in width. The upper relative stroke also lowers in this direction. The shift in the frequency of the upper peak is relatively mild, indicating that the optimized absorber is robust with respect to both frequency placement and amplitude level.

Table 3. Peak and stroke metrics at the alpha levels for the selected design (μ = 0.05).

α level	Upper peak amplitude (mm)	Upper relative stroke (mm)	Peak bandwidth (Hz)	Frequency at upper peak (Hz)
0.000	3.154	9.200	5.098	8.565
0.250	2.790	8.402	3.846	8.620
0.500	2.466	7.691	2.537	8.659
0.750	2.179	7.096	1.274	8.698
1.000	1.929	6.585	0.000	8.721

Peak bandwidth is defined here as the uncertainty-induced span of controlled-peak locations, $B\alpha = fp,max,\alpha - fp,min,\alpha$, where fp,max,α and fp,min,α are the largest and smallest frequencies at which the evaluated alpha-cut corner responses attain their controlled local maxima. It is not a conventional −3 dB bandwidth and becomes zero at $\alpha = 1$ because the alpha-cut collapses to the single nominal design. The frequency at upper peak is the frequency at which the upper response envelope reaches its maximum.

Table 3 is useful for design review because it separates nominal performance from support-wide robustness. The crisp nominal value at $\alpha = 1$ is the central peak, while the smaller alpha levels represent wider uncertainty boxes. For the inner alpha levels, the peak remains near the nominal level and the stroke remains moderate. The largest spread occurs only when the whole fuzzy support is considered. This indicates that simultaneous mistuning, damping drift and support-stiffness variation are the main drivers of the widest support peak.

4.2. Response values at selected frequencies

Typically design engineer of a company wants at least mere numbers at key speeds instead of just “a full response curve”. The displacement amplitudes in millimetres at selected frequencies are given in **Table 4**. The uncontrolled amplitude peaks at close to 9.76 Hz, and the dynamic amplification has been spread in quite short lobes by fuzzy robust design. This indicates that the fuzzy support interval is larger at frequencies of 8.79 Hz and 10.74 Hz than it is at those other two rates (i.e., at 7.81 Hz or 12.69 Hz), confirming that uncertainty in effective stiffness is concentrated near the coupled-resonance neighborhoods rather than being uniformly spread across the band as a whole.

Table 4. Selected-frequency amplitudes for the uncontrolled system, the deterministic reference, and the fuzzy robust design.

λ	Frequency (Hz)	Uncontrolled (mm)	Den Hartog (mm)	Fuzzy central (mm)	Fuzzy lower bound (mm)	Fuzzy upper bound (mm)
0.800	7.809	1.016	1.270	1.263	0.908	1.990
0.900	8.786	1.905	2.025	1.924	1.188	2.894
1.000	9.762	10.197	1.808	1.752	1.237	2.735
1.100	10.738	1.718	1.692	1.756	1.093	3.054
1.200	11.714	0.830	0.939	0.970	0.674	1.517
1.300	12.690	0.531	0.580	0.592	0.451	0.813

Table 4 is the amplitude at selected frequencies for the uncontrolled system, and the deterministic reference and fuzzy robust design. The final two fuzzy columns are the millimetre long lower and upper alpha-zero response limits.

We do this by generating a selected-frequency table that will provide us with three practical conclusions. The fuzzy robust design outperforms the uncontrolled system at all selected frequencies. Second, worst-case support is not symmetric around the natural frequency of the original system because changes in fractional damping and support stiffness alter effective coupled stiffness. Third, the deterministic Den Hartog reference yields a good performance near the nominal split peaks, but it provides no interval guarantee since it is not optimized towards fuzzy uncertainty.

The only single entry at $\lambda = 0.9$ is a local off-design effect since the deterministic Den Hartog amplitude is greater than the uncontrolled amplitude by only a small amount and does not represent global failure of the absorber. The response energy is shifted by the classical tuning towards one of the split lobes, whereas with a fuzzy robust design balanced even over the full uncertainty band just lobe heights are achieved. This is the second motivation for why peak- and envelope-based comparisons (as opposed to pointwise comparisons) are more meaningful when assessing targeted-band absorbers.

4.3. Objective map and optimum structure

Figure 3 presents the strong objective surface for mass ratio and fixed fractional order. That means the surface is smooth and vaguely convex-looking over the practical area, with a shallow valley rather than an isolated point. Therefore, this feature is beneficial for implementation, as small manufacturing errors in tuning or damping should not produce a performance loss due to immediate stiffness at the location. The design space is thus well behaved over the parametric range we examined.

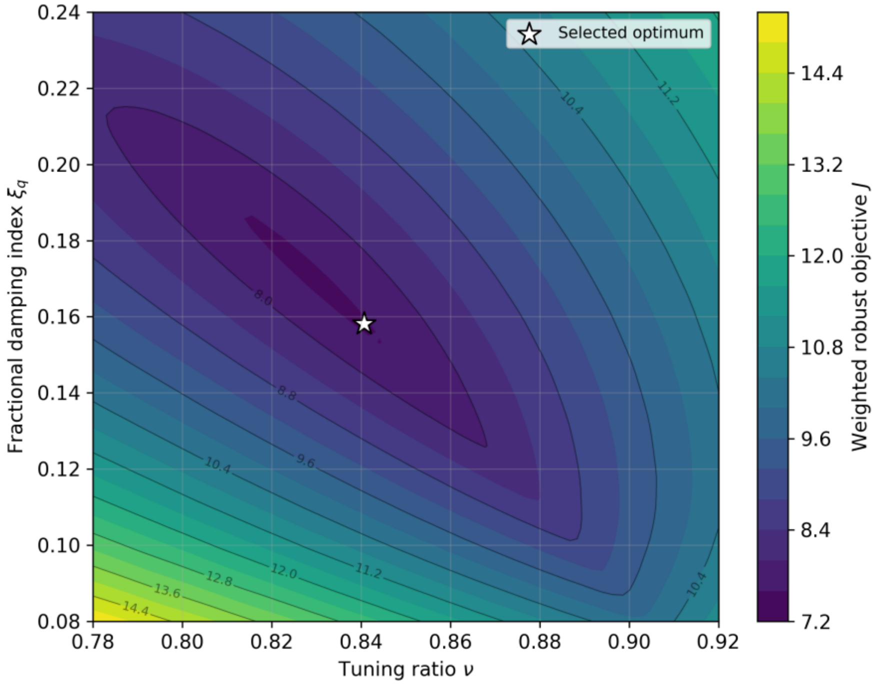

Figure 3. Robust objective map for $\mu = 0.05$ and $q = 0.58$.

These contours also explain why the optimal tuning ratio falls below the classical Den Hartog value. The fuzzy objective must balance both split peaks over the complete alpha-cut response envelope rather than match only two nominal peaks. Because the fractional damping term contributes frequency-dependent storage as well as loss, it changes the absorber's effective stiffness and damping; a slightly lower tuning ratio compensates for this shift and reduces the worst upper-envelope peak under adverse corner combinations. This behavior is reflected in the contour geometry.

The optimized parameter trends for the three mass ratios have been collected in **Figure 4**. Only 3 mass ratios were investigated but, again, the trends remain similar: the optimal tuning ratio decreases nearly linearly with μ, the optimal fractional damping index increases almost linearly and the optimal fractional order remains near 0.60. This order of timing is helpful for implementation since a single physical fractional-damping technology could be preserved with different stiffness and coefficient values depending on the mass of an absorber.

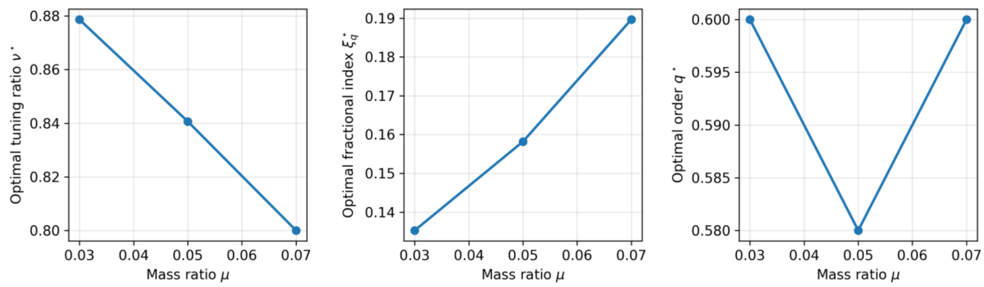

Figure 4. Parameter trends with mass ratio.

The response maps and trend plots help clarify the generalizability of the numerical results. The rotor-support oscillator absolute values as in **Table 1** are specific, but the design logic does not confine to a single set of parameters. The same procedure can be followed for any support-dominated rotating-machine mode that can be represented as an equivalent single-mode oscillator: identify the dominant mode, add the absorber ratios, specify triangular uncertainty bands, propagate alpha-cuts and minimize the weighted robust objective. The only thing that would need to be recalculated is the numerical optimum and the local surrogate coefficients for some other machine.

4.4. Alpha-cut contraction and stroke demand

Figure 5 shows the upper peak amplitude and its relative stroke vs alpha. Both curves contract consistently towards the sharp centre. It decreases from 3.154 mm at α = 0 to 1.929 mm at α = 1, and the stroke falls from 9.200 mm to 6.585 mm during this interval as well. These monotonic trends imply the nesting of corresponding support intervals in the expected way, without any nonphysical response-band crossing or inversion.

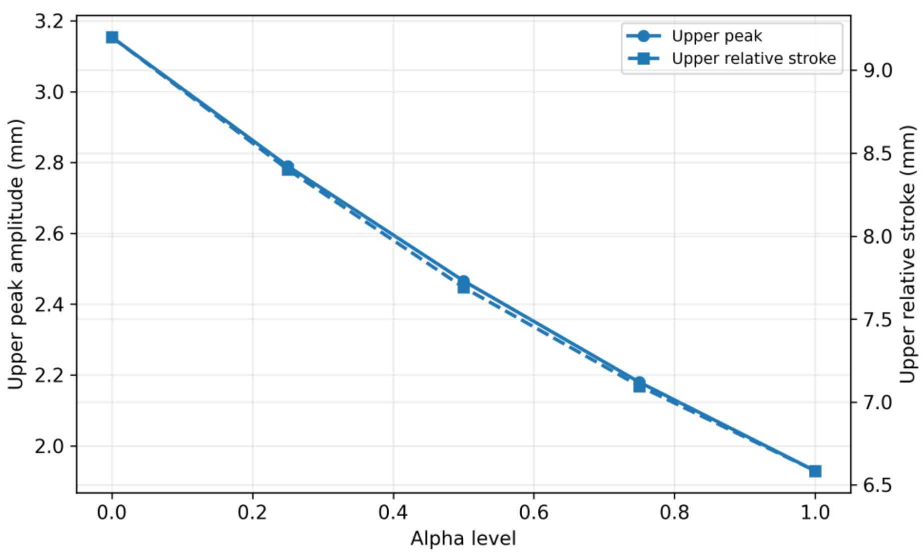

Figure 5. Alpha-cut evolution of peak amplitude and TMD stroke.

The stroke curve is notable in that it can help with the limitations from a hardware perspective. If the auxiliary travel is limited by packaging, a designer might accept a slighter larger peak. The chosen design already considers the risk/benefit trade-off in the present robust functional because there is a stroke penalty. The same framework can apply a higher stroke-penalty weight larger when the available machine space is tighter, resulting in an optimum that would differ from the previous one.

4.5. Sensitivity ranking

The local normalized sensitivities of the robust objective are listed in **Table 5** and shown in **Figure 6**.

Table 5. Local normalized sensitivities of the robust objective at the selected design.

Parameter	dJ_dtheta	Normalized_sensitivity
mu	−60.395	0.400
nu	2.416	0.269
xi	−4.452	0.093
q	0.196	0.015

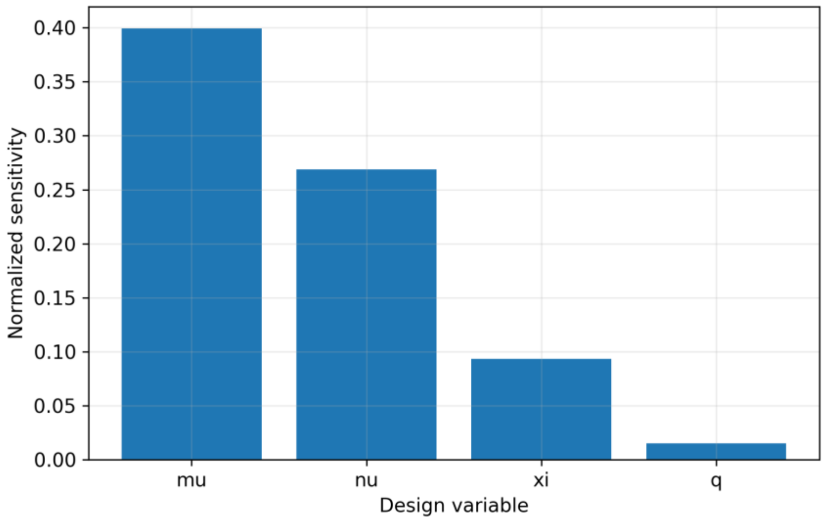

Figure 6. Local sensitivity ranking for the robust objective.

The first ranking indicates that mass ratio and tuning ratio dominate the objective, while at second level data refers that fractional damping index is secondary and finally local effect of fractional order is only little around the optimum. It does not imply that the constant order is rather irrelevant in a larger design sense, but once $q \approx 0.58$ is close to optimum, then a small local perturbation of q reduces the objective less than by the same relative (for instance by ε)% change of either μ or ν. The engineering logic is obvious: if resources for design are constrained, the first lever that should be pulled is controlling absorber mass and tuning accuracy. While response smoothness is improved by fractional-order refinement, it is not the most sensitive manufacturing variable in a selected design.

A second and equally enlightening interpretation of the sensitivity results. The bloated sensitivity w.r.t. μ does not equate to larger mass is always better; it indicates that the resistant objective mostly influenced by the available folks of absorber mass. This is reasonable since μ only appears in the coupled equations through the absorber inertia, the reconstructed spring coefficient and the fractional damping coefficient. A natural consequence of this is that the sensibility to the tuning ratio is also a measure of system detuning and it can be directly measured by the split-peak balance.

4.6. Engineering interpretation

Analysing the principal response ratio allows to interpret the campaign numerically. This is essentially a denominator-shaping problem; peak suppression can be formulated close to the coupled resonances analysed here.

$$A(\lambda) = \left| \frac{z_{22}}{z_{11}z_{22} - z_{12}^2} \right| . \tag{49}$$

The mass ratio increases the inertia of the absorber, and separates out the coupled poles. By changing the tuning ratio, we can move the split peaks to the rigth or to the left. Broadening the energy-dissipation effect through the band is facilitated by a larger fractional damping index, while a difference between real and imaginary parts of the absorber impedance is determined due to presented fractional order. The fractional term is both lossy and storage, which can also explain why the optimal robust tuning will differ from that of the conventional viscous TMD rule when the fractional order falls in between zero and one. For harmonic motion, vibration velocity scales as $\Omega|X|$ and acceleration as $\Omega^2|X|$, while a first-order radiated sound-power estimate scales with the mean-square normal surface velocity. Accordingly, the reported displacement reductions should reduce the structural source term for radiated noise, although quantitative sound-pressure prediction also requires radiation efficiency, surface geometry, and acoustic boundary conditions that are not included here. A fractional order near q = 0.58 can be approximated in hardware by a viscoelastic element with a distributed relaxation spectrum, an electromagnetic damper with frequency-shaped impedance, or an active actuator using a finite-order approximation over the design band; an ideal fractional operator over all frequencies is not assumed.

And the calculations imply a simple design route. Once the machine mode to be controlled is recognized, the designer then determines the primary natural frequency and reference displacement and operating speed band. A packaging and maximum allowable auxiliary mass based absorber mass ratio is then selected. $\mu = 0.03$ still yields significant worst-case reduction for tight packaging; $\mu = 0.05$ gives an excellent tradeoff between peak reduction and stroke demand for moderate auxiliary mass; and $\mu = 0.07$ further reduces the guaranteed peak with more auxiliary mass. First iteration and last alpha-cut refinement: The values contained in **Table 2** or the fitted surrogate relations can then have a number of guiding purposes, including the tuning ratio, fractional damping index/fractional order and their initial estimates before first refinements by the final alpha-cut.

In this particular example, a balanced feasible compromise is obtained at $\mu = 0.05$. It achieves most of the benefit offered by the heavier absorber without requiring the largest auxiliary mass. Its central crest is 1.93 mm, while its support-wide worst-case peak is 3.15 mm. The $\mu = 0.07$ design gives greater absolute peak reduction, but the $\mu = 0.05$ design remains attractive because the actual absorber mass, spring rate and travel demand are all lower.

A practical limitation of the present numerical study is that it uses a reduced single-mode representation of the rotor-support system. This is a suitable first design model when one support mode dominates the response band, but real rotating machinery can also contain gyroscopic coupling, bearing nonlinearities, shaft flexibility and speed-dependent changes in stiffness and damping. Accordingly, the model is applicable when the response is linear, one well-separated support mode dominates the 6.3–14.2 Hz target band, motions are small, and gyroscopic coupling, bearing nonlinearities, shaft flexibility, and speed-dependent coefficients are negligible; it is not valid when these effects materially alter the response. For that reason, the proposed alpha-cut design should be viewed as a transparent preliminary and mid-level design tool rather than a substitute for final finite-element or test-rig validation. Its main advantage is that the uncertainty propagation remains visible: the designer can see which part of the frequency band is sensitive, how much stroke is required and which design parameter controls the robust objective most strongly. No experimental calibration is included, so the reported reductions remain numerical predictions and require rotor test-rig validation before deployment.

The selected examples also indicate why the robust fuzzy design is useful even when deterministic tuning gives a good nominal response. A deterministic absorber can be attractive at one frequency but still lose balance when several uncertain quantities drift together. The alpha-cut envelope makes this loss of balance explicit by showing the support-wide upper response instead of only the central curve. Therefore, the design criterion is closer to the way a machine is actually commissioned: the absorber must work over a range of speeds and tolerances, not only at an ideal nominal point. This is the key practical distinction between the proposed route of notifying fuzzy-fractional tuning or even a traditional single-curve tuning rule.

The peak values in the tables should therefore be viewed relative to the response envelopes in the figures for reporting purposes. The tables provide simple numerical benchmarks, and the figures indicate if those benchmarks arise from a local pinch, a wide uncertain saw tooth or an smoothly off-resonant slope. Reading them together will help reduce the chances of overinterpretation on any single frequency value, and makes for a better engineering decision.

5. Conclusion

This study proposes and evaluates an alpha-cut robust design for a fractional-order fuzzy tuned mass damper attached to a rotating-machine support mode. The formulation combines harmonic-balance equations, dimensionless frequency-response relations, triangular fuzzy numbers, direct alpha-cut interval propagation, and a weighted robust objective. For $\mu = 0.05$, the numerical example reduces the uncontrolled 10.20 mm peak to a 1.93 mm central peak, with a 3.15 mm alpha-zero upper peak. The method also provides interpretable absorber settings, support-wide response envelopes, stroke estimates, alpha-cut contraction trends, and normalized sensitivity rankings.

The results are summarized in the next sections. By using a novel alpha-cut technique, we transparently went from uncertain design data to guaranteed vibrational envelopes without needing to assume an entire probability model. Results show that optimum tuning ratio decreased with absorber mass, while optimum fractional damping index increased with absorber mass. For the analyzed machine and uncertainty level, fractional order remained close to 0.60 indicating that retuning should be through stiffness and coefficient variations rather than by changing the fractional-damping mechanism. Sensitivity analysis identified absorber mass and tuning accuracy as the dominant sources of performance variation, providing clear manufacturing priorities for the target frequency band.

In the future, work should generalize this method in four dimensions. Experimental validation should, first be done on a rotor test rig subjected to well-controlled mistuning during support-stiffness variation and absorber-stroke measurements. Second, once more field data are accessible the triangular fuzzy assumption must be contrasted with interval type-2 fuzzy sets, probability boxes and hybrid fuzzy-probabilistic models. Third, the single-mode representation present here should be expanded to look into multi-mode rotor-bearing systems under gyroscopic coupling and speed-dependent stiffness. Fourth, hardware studies to be conducted on fractional dashpot implementations using viscoelastic, electromagnetic or smart-material devices in contexts taking into account temperature, ageing and manufacturability effects.

In summary, this mathematically compact and engineering-focused framework yields a route for robust targeted-band vibration suppression when design data of rotating-machines are uncertain but known to lie within certain bounds. The expanded dynamic determinant is provided in **Appendix A**, and additional numerical implementation details are provided in **Appendix B**.

Author contributions: Conceptualization, YN and AV; methodology, YN and TMA; software, TMA and PW; validation, AV, RJ and PW; formal analysis, YN and TMA; investigation, YN and AV; resources, TMA and PW; data curation, YN and RJ; writing—original draft preparation, YN; writing—review and editing, AV, TMA, RJ and PW; visualization, YN and TMA; supervision, AV and PW; project administration, YN and AV; funding acquisition, TMA. All authors have read and agreed to the published version of the manuscript.

Funding: This work receive no funding from any external funding agencies/ institutions.

Institutional review board statement: Not applicable.

Informed consent statement: Not applicable.

Data availability statement: The data supporting the findings of this study are available within the article.

Conflict of interest: The authors declare that they have no conflicts of interest related to the work presented.

Acknowledgment: The authors acknowledge the Gulf University for Science and Technology (GUST), Kuwait, for covering the publication fees of this article.

AI use statement: During the preparation of this manuscript, the authors used OpenAI ChatGPT solely for language refinement check. No AI tools were used for data analysis, interpretation, or generation of scientific content. All outputs were critically reviewed and edited by the authors. The authors take full responsibility for the integrity and accuracy of the work.

References

1. Zadeh LA. Fuzzy Sets. Information and Control. 1965; 8(3): 338–353. doi: 10.1016/S0019-9958(65)90241-X
2. Zadeh LA. Fuzzy Sets as a Basis for a Theory of Possibility. Fuzzy Sets and Systems. 1978; 1(1): 3–28. doi: 10.1016/0165-0114(78)90029-5
3. Dubois D, Prade H. Operations on Fuzzy Numbers. International Journal of Systems Science. 1978; 9(6): 613–626. doi: 10.1080/00207727808941724
4. Hanss M. The Transformation Method for the Simulation and Analysis of Systems with Uncertain Parameters. Fuzzy Sets and Systems. 2002; 130(3): 277–289. doi: 10.1016/S0165-0114(02)00045-3
5. Hanss M. The Extended Transformation Method for the Simulation and Analysis of Fuzzy-Parameterized Models. International Journal of Uncertainty, Fuzziness and Knowledge-Based Systems. 2003; 11(6): 711–727. doi: 10.1142/S0218488503002491
6. Moens D, Vandepitte D. A Fuzzy Finite Element Method for Frequency Response Function Analysis of Uncertain Structures. AIAA Journal. 2002; 40(1): 126–136. doi: 10.2514/2.1621
7. Giannini O, Hanss M. The Component Mode Transformation Method: A Fast Implementation of Fuzzy Arithmetic for Uncertainty Management in Structural Dynamics. Journal of Sound and Vibration. 2008; 311(3–5): 1340–1357. doi: 10.1016/j.jsv.2007.10.029
8. Adhikari S, Chowdhury R, Friswell MI. High Dimensional Model Representation Method for Fuzzy Structural Dynamics. Journal of Sound and Vibration. 2011; 330(7): 1516–1529. doi: 10.1016/j.jsv.2010.10.010
9. Balu AS, Rao BN. Efficient Explicit Formulation for Practical Fuzzy Structural Analysis. Sadhana. 2011; 36: 463–488. doi: 10.1007/s12046-011-0035-3
10. Balu AS, Rao BN. High Dimensional Model Representation Based Formulations for Fuzzy Finite Element Analysis of Structures. Finite Elements in Analysis and Design. 2012; 50: 217–230. doi: 10.1016/j.finel.2011.09.012
11. Xu M, Wang X, Qiu Z. A Dual-Layer Dimension-Wise Fuzzy Finite Element Method for Structural Analysis with Epistemic Uncertainties. Fuzzy Sets and Systems. 2019; 367: 68–81. doi: 10.1016/j.fss.2018.08.010
12. Patle BK, Hirwani CK, Singh RP, et al. Eigenfrequency and Deflection Analysis of Layered Structure Using Uncertain Elastic Properties: A Fuzzy Finite Element Approach. International Journal of Approximate Reasoning. 2018; 98: 163–176. doi: 10.1016/j.ijar.2018.04.013
13. Silva ADG, Cavalini AA, Steffen V. Fuzzy Robust Design of Dynamic Vibration Absorbers. Shock and Vibration. 2016; 2016: 2081518. doi: 10.1155/2016/2081518
14. Smith MC. Synthesis of Mechanical Networks: The Inerter. IEEE Transactions on Automatic Control. 2002; 47(10): 1648–1662. doi: 10.1109/TAC.2002.803532
15. Smith MC, Wang FC. Performance Benefits in Passive Vehicle Suspensions Employing Inerters. Vehicle System Dynamics. 2004; 42: 235–257. doi: 10.1080/00423110412331289871
16. Chen MZQ, Papageorgiou C, Scheibe F, et al. The Missing Mechanical Circuit Element. IEEE Circuits and Systems Magazine. 2009; 9(1): 10–26. doi: 10.1109/MCAS.2008.931738
17. Hu Y, Chen MZQ, Shu Z. Passive Vehicle Suspensions Employing Inerters with Multiple Performance Requirements. Journal of Sound and Vibration. 2014; 333(8): 2212–2225. doi: 10.1016/j.jsv.2013.12.016
18. Shen Y, Chen L, Yang X, et al. Improved Design of Dynamic Vibration Absorber by Using the Inerter and Its Application in Vehicle Suspension. Journal of Sound and Vibration. 2016; 361: 148–158. doi: 10.1016/j.jsv.2015.06.045
19. Ma R, Bi K, Hao H. Inerter-Based Structural Vibration Control: A State-of-the-Art Review. Engineering Structures. 2021; 243: 112655. doi: 10.1016/j.engstruct.2021.112655
20. Liu C, Chen L, Lee HP, et al. A Review of the Inerter and Inerter-Based Vibration Isolation: Theory, Devices, and Applications. Journal of the Franklin Institute. 2022; 359(14): 7677–7707. doi: 10.1016/j.jfranklin.2022.07.030
21. Bagley RL, Torvik PJ. Fractional Calculus: A Different Approach to the Analysis of Viscoelastically Damped Structures. AIAA Journal. 1983; 21(5): 741–748. doi: 10.2514/3.8142
22. Rüdinger F. Tuned Mass Damper with Nonlinear Viscous Damping. Journal of Sound and Vibration. 2007; 300(3–5): 932–948. doi: 10.1016/j.jsv.2006.09.009
23. Muresan CI, Folea S, Birs IR, et al. A Novel Fractional-Order Model and Controller for Vibration Suppression in a

Flexible Smart Beam. Nonlinear Dynamics. 2018; 93(2): 525–541. doi: 10.1007/s11071-018-4207-0
24. Xu J, Chen Y, Tai Y, et al. Vibration Analysis of Complex Fractional Viscoelastic Beam Structures by the Wave Method. International Journal of Mechanical Sciences. 2020; 167: 105204. doi: 10.1016/j.ijmecsci.2019.105204
25. Sun X, Zhu A, Yin Z, et al. Hermite Finite Element Method for a Time-Fractional Order Damping Beam Vibration Problem. Fractal and Fractional. 2023; 7(10): 739. doi: 10.3390/fractalfract7100739
26. Guo R, Meng N, Wang J, et al. Response Analysis and Vibration Suppression of Fractional Viscoelastic Shape Memory Alloy Spring Oscillator under Harmonic Excitation. Axioms. 2024; 13(11): 803. doi: 10.3390/axioms13110803
27. Das A, Banerjee A, Sahoo DR, et al. Inerter-based tuned mass dampers for response control of multi-degree-of-freedom structures subjected to wind and earthquake excitations. Structure and Infrastructure Engineering. 2026; 22(4): 624–637. doi: 10.1080/15732479.2024.2345280
28. Peng Y, Sun P. Reliability-Based Design Optimization of Tuned Mass-Damper-Inerter for Mitigating Structural Vibration. Journal of Sound and Vibration. 2024; 572: 118166. doi: 10.1016/j.jsv.2023.118166
29. Nesić N, Karličić D, Cajić M, et al. Vibration Suppression of a Platform by a Fractional Type Electromagnetic Damper and Inerter-Based Nonlinear Energy Sink. Applied Mathematical Modelling. 2025; 137: 115651. doi: 10.1016/j.apm.2024.115651
30. Sofi A, Muscolino G, Di Paola M. Reliability Analysis of Structures Controlled by External Fractional Viscoelastic Dampers with Interval Parameters. Acta Mechanica Sinica. 2023; 39: 722486. doi: 10.1007/s10409-023-22486-x
31. Yang F, Sedaghati R, Esmailzadeh E. Vibration Suppression of Structures Using Tuned Mass Damper Technology: A State-of-the-Art Review. Journal of Vibration and Control. 2022; 28(7–8): 812–836. doi: 10.1177/1077546320984305
32. Aydın Y, Bekdaş G, Nigdeli SM, et al. Adaptive Harmony Search-Based Optimization of Tuned Mass Damper Inerters under Near-Fault Earthquake Records. GeoHazards. 2025; 6(3): 56. doi: 10.3390/geohazards6030056
33. Sun P, Peng Y. Reliability-Informed Design Table for Optimizing Tuned Mass-Damper-Inerter Systems to Improve Structural Seismic Performance. Probabilistic Engineering Mechanics. 2025; 80: 103769. doi: 10.1016/j.probengmech.2025.103769
34. Cai J, Gao Q, Liu Y, et al. Control Design, Analysis, and Optimization of Fractional-Order Delayed Resonator for Complete Vibration Absorption. Journal of Sound and Vibration. 2024; 571: 118083. doi: 10.1016/ j.jsv.2023.118083
35. Jafarzadeh O, Sabetahd R, Ghasemi SAM, et al. Design of a Novel Intelligent Adaptive Fractional-Order Proportional-Integral-Derivative Controller for Mitigation of Seismic Vibrations of a Building Equipped with an Active Tuned Mass Damper. Smart Materials and Structures. 2024; 33(9): 095020. doi: 10.1088/1361-665X/ad67bc
36. Ouzizi A, Belkourchia Y, Abdoun F, et al. Vibration Suppression of Periodically Loaded Beams Using Optimized Fractional Dynamic Vibration Absorbers. Journal of Vibration and Control. 2025. doi: 10.1177/ 10775463251364512
37. Li J, Sun Y, Liu X, et al. Tuning Mechanism and Parameter Optimization of a Dynamic Vibration Absorber with Inerter and Negative Stiffness Under Delayed FOPID. Mathematics. 2025; 13(13): 2124. doi: 10.3390/ math13132124
38. Den Hartog JP. The Amplitudes of Non-Harmonic Vibrations. Journal of the Franklin Institute. 1933; 216(4): 459–473. doi: 10.1016/S0016-0032(33)90915-1
39. Aydın Y, Bekdaş G, Nigdeli SM, et al. Parameter Optimization of Tuned Mass Damper Inerter via Adaptive Harmony Search. Computer Modeling in Engineering & Sciences. 2024; 141(3): 2471–2499. doi: 10.32604/cmes.2024.056693

Appendix A

The determinant $\delta(\lambda)$ can also be decomposed to explain the coupled-peak structure under this study. Write

$$s_q(\lambda) = a_q(\lambda) + ib_q(\lambda) \tag{A1}$$

with

$$a_q(\lambda) = 2\mu\xi_q\lambda^q \cos\left(\frac{q\pi}{2}\right), \qquad b_q(\lambda) = 2\mu\xi_q\lambda^q \sin\left(\frac{q\pi}{2}\right). \tag{A2}$$

Then

$$z_{11} = \left[1 - \lambda^2 + \mu\nu^2 + a_q\right] + i\left[2\zeta_p\lambda + b_q\right] \tag{A3}$$

$$z_{22} = \left[\mu\left(\nu^2 - \lambda^2\right) + a_q\right] + ib_q \tag{A4}$$

$$z_{12} = -\left[\mu\nu^2 + a_q\right] - ib_q. \tag{A5}$$

Therefore the real and imaginary parts of the determinant are

$$\Re\delta = \Re\left(z_{11}z_{22}\right) - \Re\left(z_{12}^2\right) \tag{A6}$$

$$\Im\delta = \Im\left(z_{11}z_{22}\right) - \Im\left(z_{12}^2\right). \tag{A7}$$

If we write

$$z_{11} = u_1 + iv_1, \qquad z_{22} = u_2 + iv_2, \qquad z_{12} = u_{12} + iv_{12}, \tag{A8}$$

then

$$\Re\delta = u_1u_2 - v_1v_2 - u_{12}^2 + v_{12}^2 \tag{A9}$$

$$\Im\delta = u_1v_2 + u_2v_1 - 2u_{12}v_{12}. \tag{A10}$$

The amplitude ratio may be written as

$$A(\lambda) = \sqrt{\frac{u_2^2 + v_2^2}{(\Re\delta)^2 + (\Im\delta)^2}}. \tag{A11}$$

That means, peak suppression is keeping the denominator from getting too small through the operating band. An absorber of classical type is made of only the spring term and the imaginary viscous damping term. Our model specifies in the fractional absorber a second frequency-dependent impedance term. This helps to understand why the best robust tuning can be different from the deterministic viscous rule.

The local stationarity condition for a crisp peak at $\lambda = \lambda_p$ is

$$\frac{d}{d\lambda}A^2\left(\lambda_p\right) = 0. \tag{A12}$$

Since

$$A^2(\lambda) = \frac{u_2^2 + v_2^2}{(\Re\delta)^2 + (\Im\delta)^2}, \tag{A13}$$

the stationarity equation becomes

$$\left[\left(u_2^2 + v_2^2\right)'\right]\left[(\Re\delta)^2 + (\Im\delta)^2\right] - \left(u_2^2 + v_2^2\right)\left[(\Re\delta)^2 + (\Im\delta)^2\right]' = 0. \tag{A14}$$

This identity is not directly used in the numerical search, but clarifies why the optimum valley in **Figure 3** is smooth. The condition for peak also shifts as the coupled poles move around with respect to ν, ξ_q and q.

Appendix B. Additional notes on numerical implementation

The underlying steady-state dynamic model is two degrees of freedom, hence this is cheap in its computation.

Here, for completeness, are the key numerical settings in equation form:

$$N_\lambda = 1,000 \text{ for final curves}, \qquad N_\lambda = 180 \text{ to } 240 \text{ for the search stage}. \tag{A15}$$

$$\alpha \in \{0, 0.25, 0.50, 0.75, 1.00\} \tag{A16}$$

$$N_{corners} = 2^6 = 64. \tag{A17}$$

One practical benefit of the direct corner method is that support envelopes employed in the tables can be recovered precisely from a finite list of deterministic evaluations. The reason this transparency is necessary for journal review is because auditability of the uncertainty propagation is simply easier if all uncertain terms that could propagate uncertainty are either conditioned or specified with assumptions.